NUMERICAL ANALYSIS OF DAMPING ENHANCEMENT OF A BEAM WITH SHAPE MEMORY ALLOY FOILS BONDED

Tadashige Ikeda, Hidetaka Hattori, Yuji Matsuzaki
Department of Aerospace Engineering, Nagoya University

Keywords: *shape memory alloys, constitutive equations, damping enhancement, numerical simulation.*

Abstract

Numerical analysis of damping oscillation of a cantilever beam with shape memory alloy (SMA) foils bonded was performed, as a fundamental study on damping enhancement of a structure using SMA. A constitutive model of SMA we proposed was applied, which can capture small strain cycles and effects of strain rates in stress-strain-temperature relationship quantitatively. Beams with SMA bonded were also actually manufactured and their damping performance was measured. It was seen from both the numerical simulation and the experiment that bonding SMA was useful for the damping enhancement in some cases. Moreover, the numerical result showed that proper mechanical or/and thermal treatment of SMA may make the damping performance higher.

1 Introduction

Recently a concept of so-called smart structures was proposed, where the smart structure has functions of sensors, actuators, and processors as well, and can change its shape and mechanical properties by itself for a change in its surroundings or internal condition. This smart structure concept is expected to make structures with lighter weight, higher performance, and higher reliability, so that studies on smart structures and materials have been carried out in many aerospace, architectural, and material engineering laboratories and universities in Japan, U.S.A., and Europe.

Among the smart materials composing the smart structures, SMA is one of the most promising materials because it has functions as an actuator and a sensor based on shape memory effect and pseudoelasticity as well as enough strength and stiffness as a structural element. Moreover it is expected to be used as a damping material because of a large hysteresis loop in stress-strain relationship. Thomson *et al.* [1], Gandhi and Chapuis [2], and Boller *et al.* [3] showed the damping of a beam increased significantly with SMA wires by measurement and numerical simulation. In their research SMA wires were connected to the beam with an angle such that they vibrate with a large strain amplitude. In real situation, however, SMA may be often bonded on or embedded into a structural element, where the strain amplitude is much smaller than the previously mentioned cases. Hence we focus on the latter situation, that is, the damping enhancement of structural elements using SMA bonded on or embedded into. In particular, in this paper, we examine the damping performance of SMA foils bonded on a base structure.

In the next section, first, the constitutive model of SMA to be used is briefly shown and dynamic behavior of the cantilevered beam with a tip mass and bonded SMA foils is formulated. In section 3, the validity of the constitutive model is shown by comparing the stress-strain relationships of a SMA wire measured and predicted by the model, and then the effectiveness of bonding SMA on the damping enhancement is examined by both the experiment and the numerical simulation.

2 Modeling Beam with a Tip Mass and SMA Foils Bonded

2.1 Constitutive Model of SMA

Deformation behavior of SMA is based on phase transformation and it changes significantly due to a change in thermomechanical parameters. Therefore to apply SMA to the smart structural element we must understand its behavior and present a simple yet accurate theoretical model for optimal design. When we use SMA bonded on or embedded into a base material as a damping material, effects of strain rate and small strain cycles are important, because the eigenfrequency of the structure depends on its stiffness and configuration and that the strain range of the base material is usually less than 1 %, which is much smaller than the strain range of SMA.

After investigating the published models with respect to the strain rate effects and the small strain cycles, we found there were few available models. Therefore we proposed a new constitutive model of SMA which can treat the strain rate effects and the small strain cycles [4, 5].

2.1.1 Transformation Criterion

Following Ikeda et al. [4, 5], the phase transformation criterion of SMA is given by

$$\frac{1}{2}\sigma^2\left(\frac{1}{E_M}-\frac{1}{E_A}\right)+\sigma(\varepsilon_M-\varepsilon_A)+\Delta s(T-T_0) = \Psi(z), \quad (1)$$

where σ, E_M, E_A, ε_M, ε_A, Δs, T, T_0, and z denote the stress of the material, the Young's moduli of martensitic phase and austenitic phase, the intrinsic strains of the two phases, the entropy difference between the two phases, the material temperature, the transformation temperature without dissipation, and the martensitic volume fraction. The left-hand side of the equation is the thermodynamic driving energy for the phase transformation, and the right-hand side, Ψ, is the required transformation energy (RTE). When the driving energy becomes equal to RTE, the phase transformation is assumed to take place.

The boundary RTE for the complete phase transformation can be easily estimated from experimentally measured data and is assumed approximated by

$$\Psi(z,\dot{z})=\begin{cases}\Psi_f(z) & \dot{z}>0\\ \Psi_r(z) & \dot{z}<0\end{cases}, \quad (2)$$

where $\dot{z}$ is the time derivative of the martensitic volume fraction.

To express the partial transformation cycles, we proposed a new partial transformation model, named the shift-skip model, where RTE is rewritten in the following form;

$$\Psi(z,\dot{z},z_{f,i},z_{r,i};i=0,1,\cdots,N_s) = \begin{cases}\Psi_f(z-z_{r,Ns}) \\ \quad for\ \dot{z}>0 \text{ and } z_{r,Ns}\le z<z_{f,Ns} \\ \Psi_f(z-z_{r,k-1}) \\ \quad for\ \dot{z}>0 \text{ and } z_{f,k}\le z<z_{f,k-1},\ k=1,2,\cdots,Ns \\ \Psi_r(z+(1-z_{f,Ns})) \\ \quad for\ \dot{z}<0 \text{ and } z_{r,Ns-1}\le z<z_{f,Ns} \\ \Psi_r(z+(1-z_{f,k-1})) \\ \quad for\ \dot{z}<0 \text{ and } z_{r,k-2}\le z<z_{r,k-1},\ k=2,3,\cdots,Ns\end{cases}. \quad (3)$$

Ψ_f and Ψ_r denote the boundary RTE for forward and reverse transformations, respectively. N_s is the turn number to be considered. $z_{f,i}$ and $z_{r,i}$ are a pair of memorized volume fractions of the i-th turn for forward and reverse transformation and $z_{f,0} = 1$ and $z_{r,0} = 0$. Moreover, when the specimen is loaded until $z > z_{f,k}$ or when the specimen is unloaded until $z < z_{r,k}$, the memory pairs of $z_{f,i}$ and $z_{r,i}$ with $i \ge k$ are cleared. Here, it is noted that $z_{r,Ns}$ does not exist and is not also used when $\dot{z}<0$.

2.1.2 Strain Equation

Strain is assumed to consist of elastic, transformation, and thermal parts, and is given by

$$\varepsilon=\frac{\sigma}{E_I}+(1-z)\varepsilon_A+z\varepsilon_M+\alpha(T-T_s), \quad (4)$$

where

$$\frac{1}{E_I} = (1-z)\frac{1}{E_A} + z\frac{1}{E_M}. \qquad (5)$$

α and T_s are the thermal expansion coefficient and the surrounding temperature.

2.1.3 Heat and Energy Flow Equation

Forward transformation is exothermic whereas the reverse one is endothermic. Moreover, the dissipation energy due to the internal friction changes into heat and the heat generated in the material is exchanged with the surroundings. Consequently, since temperature of SMA increases and decreases during the deformation, we must consider the heat and energy flow equation;

$$C\dot{T} + h\frac{A}{V}(T - T_s) = \left(-\Delta s T + \Psi(z, \dot{z}, z_{f,i}, z_{r,i})\right)\dot{z} - \alpha T\dot{\sigma}. \qquad (6)$$

C, h, A, and V denote the specific heat capacity at constant stress, the convection heat transfer coefficient, the exposed area, and the volume, respectively.

2.2 Beam Model

Next we formulate the beam with a tip mass and SMA foils bonded using Bernoulli-Euler beam theory.

2.2.1 Bernoulli-Euler Beam Equation

Equation of motion of Bernoulli-Euler beam is

$$\mu\frac{\partial^2 w}{\partial t^2} + \frac{\partial^2}{\partial x^2}\left(E^* I\frac{\partial^2 w}{\partial x^2}\right) = f(x,t). \qquad (7)$$

x, t, μ, w, and f denote the longitudinal coordinate, the time, the mass per unit length, the displacement, and the distributed external force. E^*I is the complex bending stiffness of the beam and given by

$$E^* I = E^*_{Al}\frac{BH_{Al}^3}{12} + 2E^*_{Ep}\frac{BH_{Ep}^3}{12} + \frac{B}{2}E^*_{Ep}H_{Ep}(H_{Al} + H_{Ep})^2, \qquad (8)$$

where E^*, B, H, and subscripts Al and Ep are the complex Young's modulus, the breadth, the thickness, and the quantities of the aluminum beam and the epoxy adhesive.

Assuming that the displacement is separable in space and time, and that the first mode vibration is dominant, that is,

$$w(x,t) = q(t)W(x), \qquad (9)$$

we obtain the following ordinary differential equation;

$$\frac{d^2 q}{dt^2} + \eta\frac{\Omega^2}{\omega}\frac{dq}{dt} + \Omega^2 q = Q, \qquad (10)$$

where q and W denote the generalized coordinate and the first modal function normalized as

$$\int_0^L \mu W^2(x)dx = 1. \qquad (11)$$

ω, η, Ω, and L are the angular frequency, the damping factor, the natural angular frequency, and the length of the beam.

$$Q(t) = \int_0^L f(x,t)W(x)dx \qquad (12)$$

is the generalized force associated with q.

2.2.2 Effect of Tip Mass

Effect of the tip mass is considered as the external force given by

$$Q_{mass} = \int_0^L -M\frac{\partial^2 w(t,L)}{\partial t^2}\delta(x-L)W(x)dx = -MW^2(L)\frac{d^2 q}{dt^2}, \qquad (13)$$

where M and δ denote the mass of the tip mass and the Dirac delta function.

2.2.3 Transmission of Force from SMA

The force from the SMA foil is assumed transmitted as if the concentrated forces act at the edges of the beam. Here we consider only a bending moment and ignore an axial force. The bending moment can be transformed into the equivalent coupling forces f_{SMA} with a distance

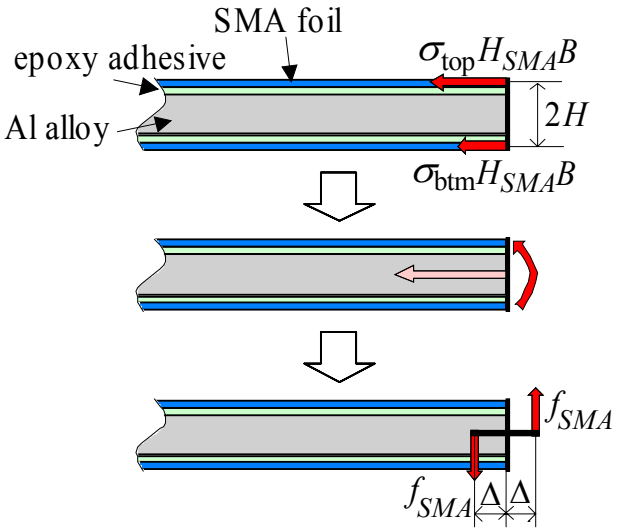

Fig. 1. Coupling forces equivalent to a bending moment due to SMA foils

of 2Δ as shown in Fig. 1 and given by the following equation.

$$\lim_{\Delta \to 0} f_{SMA}(2\Delta) = (\sigma_{top} - \sigma_{btm}) H H_{SMA} B , \tag{14}$$

where

$$H = \frac{1}{2} H_{Al} + H_{Ep} + \frac{1}{2} H_{SMA} . \tag{15}$$

The subscripts *top*, *btm*, and *SMA* are the quantities of the top foil, the bottom foil, and SMA foil. Accordingly, the generalized force generated by the SMA foils is obtained as

$$\begin{aligned} Q_{SMA} &= \lim_{\Delta \to 0} \int_0^{L+\Delta} f_{SMA} \{\delta(x - L - \Delta) \\ &\quad - \delta(x - L + \Delta)\} W(x) dx \\ &= (\sigma_{top} - \sigma_{btm}) H H_{SMA} B \frac{dW(L)}{dx} . \end{aligned} \tag{16}$$

2.2.4 Relationship between Displacement and Strain of SMA Foils

The strain of the top SMA foil is obtained, by integrating the local strain over the beam and by considering the boundary condition, as

$$\begin{aligned} \varepsilon_{top} &= \varepsilon_{pre} - \frac{1}{L} \int_0^L \frac{d^2 W}{dx^2} qH dx \\ &= \varepsilon_{pre} - \frac{1}{L} \left\{ \frac{dW(L)}{dx} \right\} qH , \end{aligned} \tag{17}$$

Table 1 Constants of the wire and surroundings

Constant	Value
d	0.75 mm
E_A	43.3 GPa
E_M	22.9 GPa
ε_A	0.0
ε_M	0.0304
α	1.04×10^{-5} 1/K
Δs	-0.246 MJ/(m^{3}K)
C	2.97 MJ/(m^{3}K)
T_0	248.6 K (small loop)
	243.4 K (frequency effect)
T_s	291.2 K (small loop)
	296.5 K (frequency effect)
h	43.4 W/(m^{2}K)
A/V	5.33×10^3 1/m
Ψ_c	2.81 MJ/m^3
a_1	1.0×10^{10}
a_2	1.0×10^6

where ε_{pre} is the prestrain when the foil is bonded. The bottom strain is obtained in a similar way as

$$\varepsilon_{btm} = \varepsilon_{pre} + \frac{1}{L} \left\{ \frac{dW(L)}{dx} \right\} qH . \tag{18}$$

3 Results and Discussion

3.1 Validity of the Constitutive Model of SMA

First we examined the validity of the proposed constitutive model of SMA by comparing predicted stress-strain relationship with measured data. In particular, the effects of small strain loops and loading frequencies were examined, because these effects are important when SMA is bonded on or embedded into the base structural element as a damping material. A NiTi SMA wire was used as a specimen.

RTE was estimated from the experimental data as

$$\begin{cases} \Psi_f = \Psi_c \left[1 + \left\{ -a_1^{-z} + a_2^{-(1-z)} \right\} \right] \\ \Psi_r = \Psi_c \left[-1 + \left\{ -a_1^{-z} + a_2^{-(1-z)} \right\} \right] \end{cases}, \tag{19}$$

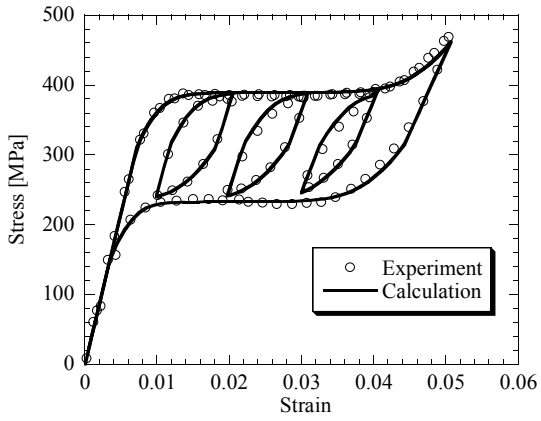

Fig. 2. Comparison of small strain loops between the experiment and the calculation

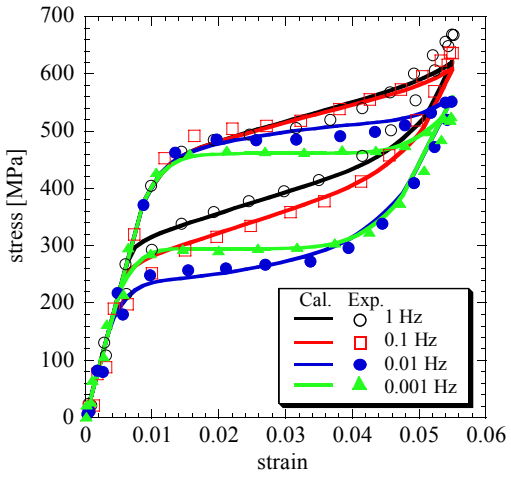

Fig. 3. Comparison of the effect of loading frequency between the experiment and the calculation

where Ψ_c, a_1, and a_2 were the material constants. The parameters of the wire and surroundings used in the numerical simulation are listed in Table 1.

Fig. 2 and 3 show comparison of stress-strain relationship between calculation and experiment on the effects of small strain loops and loading frequencies, respectively. The symbols are the measured data and the curves are the prediction. It is seen from Fig. 2 that the proposed model can capture the features of the measured boundary and inner small hysteresis loops quite well. This result indicates that RTE approximated by a sum of two exponential functions and the shift-skip partial transformation model are reasonable. From Fig. 3, the model can capture also the loading

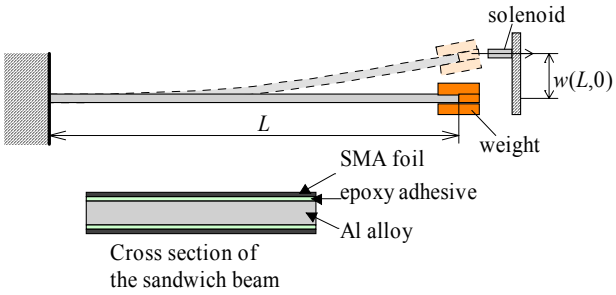

Fig. 4. Schematic of the cantilever beam used in the experiment and a cross section of the beam with SMA foils bonded

frequency effect from 0.001 Hz to 1 Hz. Moreover, we made sure that almost adiabatic deformation took place at a loading frequency of more than 1 Hz and the stress-strain loops did not change much.

3.2 Damping Vibration of Beams with SMA

Fig. 4 shows a schematic figure of the cantilevered beam used in the damping enhancement measurement and a cross-section of the beam with SMA foils bonded on its surfaces. Five specimens were made. Those were a just aluminum beam (Al), aluminum beams with bonded SMA foils in R phase at room temperature (Al+R), with bonded SMA foils in austenitic phase (Al+A), with bonded prestrained SMA foils (Al+PA), and with bonded stainless steel foils (Al+S). The prestrain was applied to the austenitic SMA foils expecting SMA to vibrate around the center of the boundary stress-strain loop. The stainless steel foil was used to compare SMA foil with another metal foil. To avoid the effect of aerodynamic damping, the experiment was performed in a vacuumed camber. In the experiment the beams were first bent by quasistatically pulling their free end and then released to start a vibration. The vibration was measured by a strain gauge attached at 30mm from the clamp on the beam.

Fig. 5a shows the envelopes of the positive side of the measured damping vibration of the beams. The damping of Al+R, indicated by a blue colored line, is approximately 200 % superior when compared to Al, indicated by the black line, and is approximately 100% superior

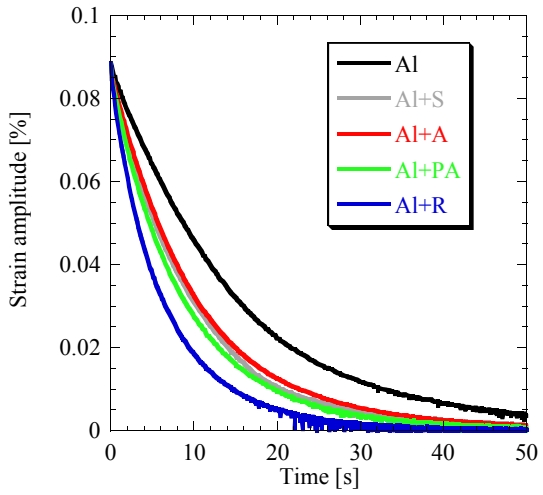

Fig. 5a. Measured envelope of damping vibration wave

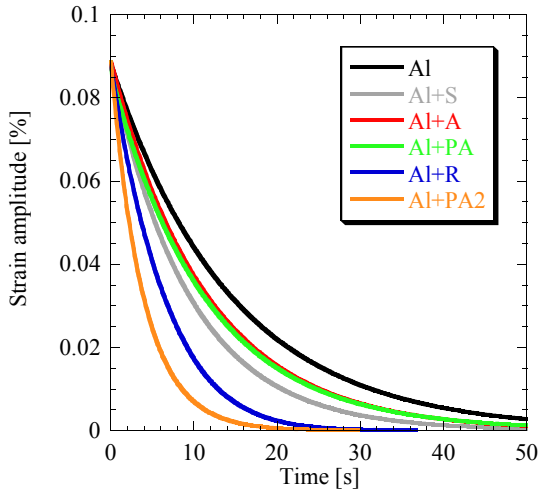

Fig. 5b. Predicted envelope of damping vibration wave

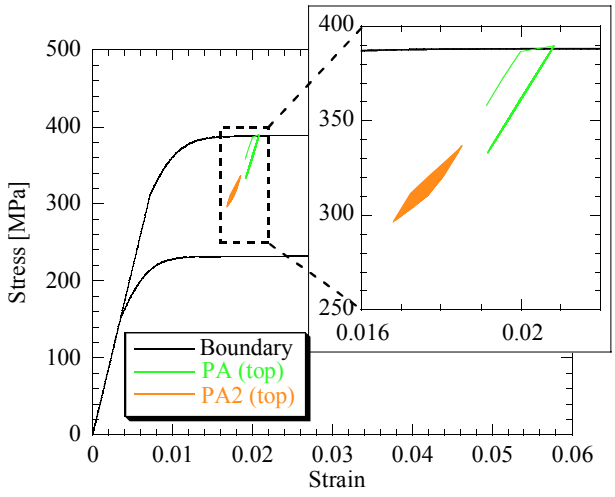

Fig. 6. Stress-strain relationship of the top SMA foil

Table 2 Constants of the aluminum beams, the epoxy adhesive layer, the stainless steel foil, the SMA foils and the surroundings

Constant	Value
L	200 mm
B	20 mm
H_{Al}	2 mm
H_{Ep}	0.08 mm
H_R	0.04 mm
H_A	0.05 mm
H_S	0.04 mm
E_{Al}	73.0 GPa
E_{Ep}	4.64 GPa
E_R	26.7 GPa
$E_A \leftrightarrow E_M$	43.3 GPa ↔ 22.9 GPa
E_S	200 GPa
η_{Al}	0.002546
η_{Ep}	0.06136
η_S	0.003501
μ_{Al}	0.1040 kg/m
μ_{Ep}	0.0038 kg/m
μ_R	0.0090 kg/m
μ_A	0.0112 kg/m
μ_S	0.0126 kg/m
ε_{pre}	0.02
M	144.6 g
α	1.04×10^{-5} 1/K
C	2.97 MJ/(m^{3}K)
T_s	291.2 K
h	43.4 W/(m^{2}K)
$\varepsilon_A \leftrightarrow \varepsilon_M$	0.0↔0.0304
Δs	–0.246 MJ/(m^{3}K)
T_0	248.6 K
Ψ_{Ac}	2.81 MJ/m^3
a_{A1}	1.0×10^{10}
a_{A2}	1.0×10^{6}
A/V_A	2.0×10^{4} 1/m
$\varepsilon_{R+} \leftrightarrow \varepsilon_{R-}$	0.042↔-0.042
Ψ_{Rc}	9.9 MJ/m^3
a_{R1}	1.0×10^{4}
a_{R2}	1.0×10^{4}
A/V_R	2.5×10^{4} 1/m

when compared to Al+S, indicated by the gray line. Damping performance of Al+A and Al+S are similar and Al+PA is a little better than those.

From this result the material parameters of aluminum beam and epoxy adhesive were estimated. With respect to the material constants for the SMA foils, we assumed that they were the same as those for the wire used in the preliminary experiment etc. Moreover, it was assumed that rearrangement between R+ phase and R- phase took place in the R phase foils. The material constants of the aluminum beam, the epoxy adhesive, and the foils are listed in Table 2, where the subscripts *S*, *R*, *R*+, and *R*- denote the quantities on the stainless steel, R phase SMA, R+ and R- phase, respectively. Accordingly, qualitative comparison of damping performance was made between the prediction of damping vibration of the beams with SMA foils and the corresponding experiment.

Fig. 5b shows the envelopes of the positive side of the calculated damping vibration of the beams. The simulated result seems to be in qualitatively good agreement with the experiment, although the damping of Al+PA is less than Al+S, being different from the experiment.

It can be seen form Fig. 5 that bonding R phase SMA is effective for the damping enhancement and that the modeling of the beam with a tip mass and SMA foils bonded is reasonable.

3.3 Effect of prestrain of SMA

The austenitic SMA foils were prestrained because we expected SMA to vibrate around the center of the boundary stress-strain loop. However, we could not obtain a good damping enhancement for Al+PA beam, where the austenitic SMA foils were stretched by 2% and bonded on the aluminum beam. Since the damping performance relates to the area of the stress-strain loop, we examined the area for Al+PA beam in the simulation. Green curve in Fig. 6 illustrates the stress-strain relationship of the top SMA foil of Al+PA beam during the vibration. It was found that we could not obtain a large hysteresis loop in this condition because the deformation of SMA foil was in an elastic range and no transformation took place. Therefore, we tried simulating vibration of a beam with SMA foils which were stretched and relaxed a little before bonded so as to actually vibrate around the center of the hysteresis loop (Al+PA2). Orange curve in Fig. 5b illustrates the envelope of the simulated damping vibration of Al+PA2 beam. In this beam we could obtain a damping performance as good as Al+R beam. At this time the area of the stress-strain relationship became larger as shown with the orange curve in Fig. 6.

4 Conclusion

Effects of SMA on damping enhancement was examined. To this end first a new constitutive model of SMA for partial transformation cycles was proposed. Next a beam with a tip mass and bonded SMA foils was formulated. The comparison of simulated stress-strain relationships for SMA wire with measured data showed the validity of the SMA model. Finally beams with SMA foils bonded were manufactured and we measured their damping vibration and simulated them using the formulated beam model. The predicted and measured waves of the damping vibration were in qualitatively good agreement with each other. The results showed that bonding R phase SMA was effective for damping enhancement and bonding austenitic SMA might increase damping performance by giving proper mechanical or/and thermal treatment.

As future works we must measure the mechanical property of SMA foils to confirm the validity of the model more and make a beam with optimally prestrained austenitic SMA foils bonded to verify the prediction.

Acknowledgements

A part of this research was conducted as “R&D on Smart Materials and Structure Systems” project within the Academic Institutions Centered Program collaborated with RIMCOF (R&D Institute of Metals and Composites for Future Industries) supported by NEDO (the New Energy and Industrial Technology Development Organization) that is supervised

by METI (the Japanese Ministry of Economy, Trade and Industry). The authors would like to thank Mr. Toshiyuki Sasaki for his help in the experiment.

References

[1] Thomson P, Balas G J and Leo P H. The use of shape memory alloys for passive structural damping, *Smart Mater. Struct,*.Vol. 4, pp. 36-42, 1995.

[2] Gandhi F and Chapuis G 2001 Passive damping augmentation of a vibrating beam using pseudoelastic shape memory alloy wires *Proc. 11th Int. Conf. Adapt. Struct. Tech.*, Nagoya, pp. 319-335, 2001.

[3] Boller C, Konstanzer P, Matsuzaki Y and Ikeda T. Damping with Shape Memory Alloys for Structural Systems, *Proc. 11th Int. Conf. Adapt. Struct. Tech.*, Nagoya, pp. 336-343, 2001.

[4] Ikeda T, Nae FA and Matsuzaki Y. Macroscopic constitutive model of shape memory alloys for partial transformation cycles. *Proc SPIE Smart Struct. Mater. 2004,* San Diego, Vol. 5383, 2004, at press.

[5] Ikeda T, Nae FA, Naito H and Matsuzaki Y. Constitutive model of shape memory alloys for unidirectional loading considering inner hysteresis loops, *Smart Mater. Struct.*, 2004, at press.